光学学报

上波导层In摩尔分数对InGaN基蓝光激光器性能研究

付星瑞，李书平*

厦门大学物理科学与技术学院，福建 厦门 361005

摘要 基于实验样品结构，利用PICS3D模拟软件，构建了具有同样结构的InGaN基蓝光激光器，并采取了与实验样品一致的内部参数测定方式，结果表明，内部损耗相对误差为3.5%，实现了严格的比对。随后，构建了一系列InGaN基蓝光激光器，通过比较不同In摩尔分数下的光输出功率、载流子分布、光场分布、辐射复合系数和能带曲线等参数，对上波导层中的In摩尔分数进行优化研究。设计得到了光功率更优的两种不同的优化结构，均有效减少了电子泄漏，提高了斜率效率，从而有效提高了光电转化效率，其中渐变In摩尔分数上波导层结构提升效果更为显著。

关键词 二极管激光器；上波导层；渐变层；电子泄漏

中图分类号 TN248 **文献标志码** A **DOI：** 10.3788/AOS230773

1 引 言

近年来，由于InGaN基激光二极管（LD）具有成本低、尺寸小、效率高和寿命长等特性，在显示、照明、检测、激光加工和水下通信等方面都有了广泛的应用[1-4]。而随着应用范围的推广，其对激光器性能的要求也随之增加。由于迁移率的差异，空穴的注入速度会慢于电子，在几个量子阱中空穴的注入量各不相同，因此过多的电子会溢出量子阱泄漏至p型区，而靠近n侧的量子阱内缺少空穴，辐射复合率也因此降低[5]。此外，InGaN材料本身的极化效应会导致能带倾斜，造成量子限制斯塔克效应[6]。因此，为抑制极化效应和电子泄漏，研究人员提出许多优化结构。Park等[7]尝试使用与GaN晶格匹配的四元AlInGaN势垒，显著增强了激光器的光学增益。Liu等[8]调整第一层势垒的掺杂增强了量子阱的捕获效果，提高了辐射复合率。Liang等[9]直接移除了多量子阱（MQW）中第一层势垒，降低了电子势垒，提高了电子注入率，同时减少了光学损耗。Yang等[10]研究了最合适的下波导层In摩尔分数。Liang等[11]进一步提出了高In组分第一层量子垒与下波导层的新型结构，减小了光学损耗。Onwukaeme等[12]得到了蓝光LD中最合适的Mg掺杂浓度。Xing等[13]优化电子阻挡层（EBL）的Al组分来抑制电子泄漏，He等[14]提出超晶格EBL，减缓了能带弯曲，提高了空穴注入。杜小娟等[15]研究了四元渐变AlInGaN EBL，在普通四元EBL的基础上提升了电光转化效率等。

本文初始结构参照Hu课题组的LD器件[16]，使用PICS3D模拟软件构建了边发射InGaN基蓝光LD模型，为进一步提高LD器件的光电性能，对上波导层In摩尔分数尝试优化，对其光电特性、能带结构、光场分布、复合率分布等计算分析，得到了效果最优的两种优化结构。

2 结构与参数

本文进行模拟计算时所采用的蓝光LD结构示意图如图1所示，初始结构A基于参考文献的LD器件[16]，器件结构从下至上依次为：30 μm厚的GaN衬底，且加入硅（Si）的n型掺杂，浓度为2×10^{18} $\mathrm{cm^{-3}}$；2 μm厚的n型GaN层，掺杂浓度为1×10^{19} $\mathrm{cm^{-3}}$；1.4 μm厚的n型$\mathrm{Al_{0.08}Ga_{0.92}N}$下覆盖层，掺杂浓度为$2\times10^{18}$ $\mathrm{cm^{-3}}$；0.25 μm厚的n型$\mathrm{In_{0.04}Ga_{0.96}N}$下波导层，掺杂浓度为$2\times10^{18}$ $\mathrm{cm^{-3}}$；有源区为两个周期的MQW，由3个厚度为6.7 nm的非故意掺杂GaN势垒和2个厚度为2.5 nm的非故意掺杂$\mathrm{In_{0.16}Ga_{0.84}N}$势阱构成；上波导层为0.25 μm厚的p型$\mathrm{In_{0.02}Ga_{0.98}N}$，掺杂浓度为$1\times10^{18}$ $\mathrm{cm^{-3}}$；接下来是p型EBL，为20 nm厚的$\mathrm{Al_{0.2}Ga_{0.8}N}$，掺杂浓度为$1\times10^{18}$ $\mathrm{cm^{-3}}$；p型覆盖层为40个周期的超晶格结构，垒层为2.5 nm厚的$\mathrm{Al_{0.07}Ga_{0.93}N}$，阱层为2.5 nm厚的GaN，掺杂浓度均为$1\times10^{18}$ $\mathrm{cm^{-3}}$；最后是50 nm厚的p型InGaN接触层，前40 nm为$\mathrm{In_{0.02}Ga_{0.98}N}$，掺杂浓度为$5\times10^{18}$ $\mathrm{cm^{-3}}$，最后

收稿日期：2023-04-04；**修回日期**：2023-04-24；**录用日期**：2023-05-24；**网络首发日期**：2023-06-28

通信作者：*lsp@xmu.edu.cn

10 nm 为更好地实现欧姆接触，采用掺杂浓度为 1×10^{19} cm^{-3}的 $In_{0.04}Ga_{0.96}N$。表 1 归纳了以上不同层所对应的掺杂浓度，标准结构 A 与优化结构 B、C 的掺杂浓度完全一致，优化结构 B 和 C 的上波导层分别为 $In_{0.08}Ga_{0.92}N$ 和渐变的 $In_{0.05\text{-}0.08}Ga_{0.95\text{-}0.92}N$，其余结构部分均与 A 相同。

整个器件的腔长为 1200 μm，脊宽为 15 μm。谐振腔的端面反射率为 0.05 和 0.99[17]，分别对应增透膜和高反射薄膜。GaN 外延层生长方向为(0001)晶向，模拟计算中，俄歇复合系数根据相关实验数据设为 1×10^{-31} cm^6/s[18]，肖特基-瑞利-霍尔(SRH)复合时间设为 1.5 ns[19]，其他吸收系数设置为 0[20]。设定量子阱结区温度为 460 K，由于表面电荷可能被屏蔽，使用了 Fiorentini 模型[21]，考虑到缺陷对内置极化的部分补偿，将屏蔽因子设为 30%[22]。InGaN 材料的能带偏移率(O_{ff})设为 0.65[23]。此外，关于材质相关的参数如表 2[24-25]所示，模拟计算中的其他参数可查阅文献[26]。

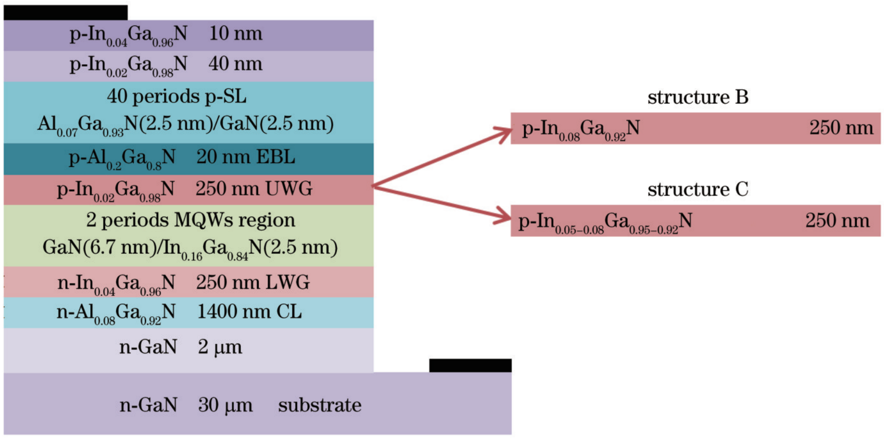

图 1　InGaN 基 LD 标准结构与新结构示意图

Fig. 1　Schematic diagram of InGaN-based LD standard structure and new structures

表 1　InGaN 基 LD 标准结构掺杂浓度

Table 1　Doping concentration of InGaN-based LD standard structure

Layer	Doping concentration /(10^{18} cm^{-3})
$In_{0.04}Ga_{0.96}N$ P++	10 (Mg)
$In_{0.02}Ga_{0.98}N$ P	5 (Mg)
40 periods SL	1 (Mg)
$Al_{0.2}Ga_{0.8}N$ EBL	1 (Mg)
$In_{0.02}Ga_{0.98}N$ UWG	1 (Mg)
2 periods MQWs	0
$In_{0.04}Ga_{0.96}N$ LWG	2 (Si)
$Al_{0.08}Ga_{0.92}N$ CL	2 (Si)
GaN N	10 (Si)
GaN Substrate	2 (Si)

表 2　GaN、AlN 和 InN 的材质参数

Table 2　Material parameters for GaN, AlN, and InN

Sample	InN	GaN	AlN
Lattice constant /(10^{-10} m)	3.548	3.189	3.112
Lattice mismatch /%	11	0	−2.4
Refractive index	3.4167	2.5067	2.0767
Energy bandgap /eV	0.684	3.358	6.032
Bond strenth /eV	1.93	2.20	2.88

图 2 展示了该仿真结构得到的光功率模拟结果与参考文献中相似结构的对比图，两者趋势基本一致，文献[16]实验得到的激射波长为 445 nm，本文模拟得到的激射波长同样为 445 nm，与之一致。

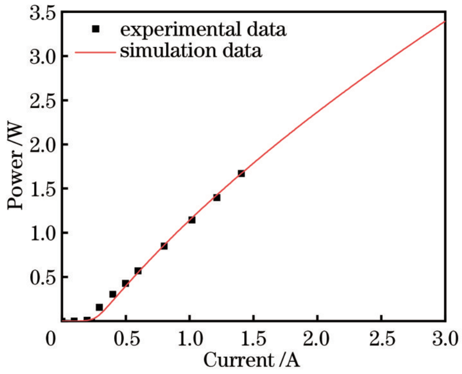

图 2　标准结构的模拟和实验光功率-电流特性曲线

Fig. 2　Simulation and experimental *L*-*I* characteristic curves of standard structure

此外，本文尝试了参考文献中提到的变腔面反射率法来估算内部损耗与载流子注入率，如图 3(a)所示。激光器内部光学损耗(α_i)与载流子注入效率(η_{inj})决定了激光器的斜率效率(SE)，计算公式[27]为

$$\frac{1}{R_{SE}} = \frac{q}{hc\eta_{inj}}\left(1+\alpha_i\frac{1}{\alpha_m}\right), \tag{1}$$

式中：q 为电子电荷；h 为普朗克常数；c 为光速；α_m 为激光器的腔面损耗。将前腔面反射率分别为 10%、45%、82% 的激光器的斜率效率代入式(1)拟合，如图

3(b)所示，可以得到内部损耗为6.56 cm^{-1}，载流子注入效率为95%，相比参考文献[16]实验结果的6.8 cm^{-1}、90%，相对误差分别为3.5%、5.3%，证明了本文模拟结果的可靠性。

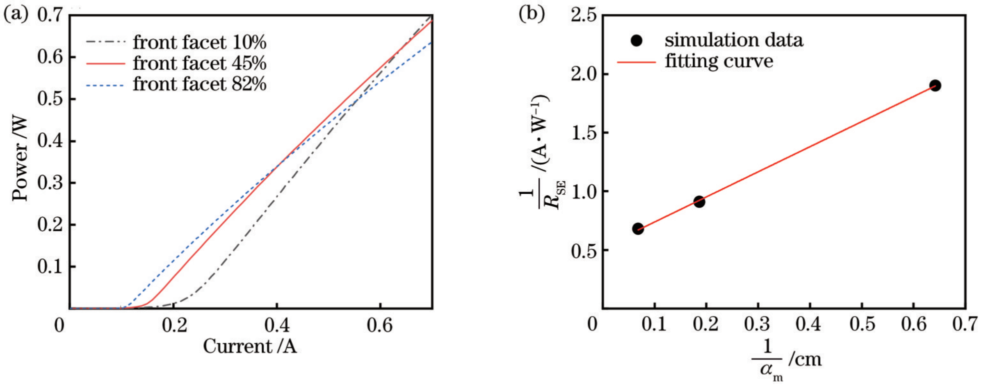

图 3 蓝光激光器内部参数。(a)三种不同前腔面反射率下的L-I曲线；(b)通过镜面损耗和斜率效率拟合内部光学损耗和载流子注入效率的曲线

Fig. 3 Internal parameters of blue laser. (a) Three P-I curves with different front facet coating reflectivities; (b) curve of internal optical loss and carrier injection efficiency obtained by fitting mirror loss and slope efficiency

3 初始结构优化结果

图4(a)为标准结构(以下简称结构A)的光电转化效率(PCE)与注入电流关系曲线，随着电流的增加，PCE先迅速升高再缓慢降低，这是由于激光器的损耗随着注入电流增加，功率随之饱和。可以看出，在0.8～1.5 A之间光电转化效率在23%以上，为较良好的工作区域，其中1 A处为转化效率最高点，后续将工作电流选取在这一区域下测试。图4(b)为1 A注入电流下样品A的电子电流密度与载流子浓度对数曲线，可以看出，在上波导层处仍有4200 A/cm^{2}的电子电流，说明电子从量子阱中溢出过多，电子泄漏严重。因此本文将针对上波导层探究优化结构，提升电子阻挡能力，减少上波导层的非辐射复合。

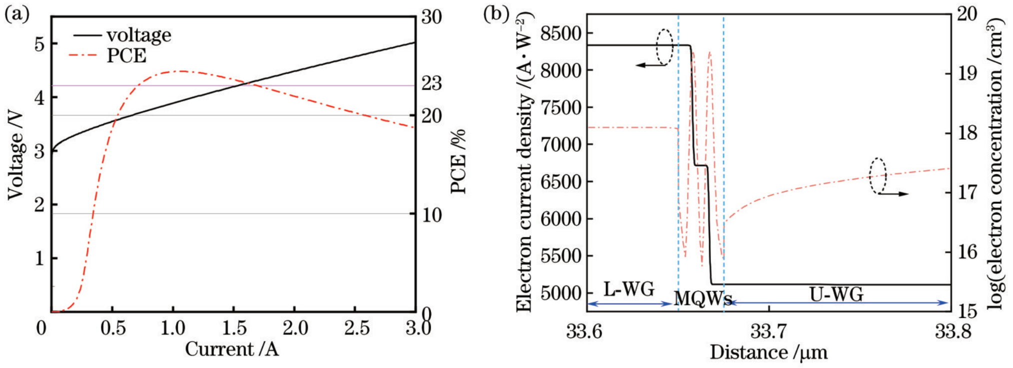

图 4 标准结构性能。(a)光电转化效率和电压与注入电流的关系曲线；(b)1 A电流下的电子电流密度曲线与电子浓度对数曲线

Fig. 4 Performance of standard structure. (a) Curves of photoelectric conversion efficiency and volt-ampere characteristic; (b) electron current density curve and logarithmic curve of electron concentration at 1 A current

在三元化合物中，可以通过调节In和Ga的比例来改变带隙，相应地改变导带和价带，从而提高电子势垒，阻碍电子泄漏。本文在样品A的基础上，尝试对上波导层In摩尔分数进行优化。首先构建了一系列不同In摩尔分数上波导层的蓝光LD器件，其他参数与样品A均相同，取不同样品在0.8 A与1 A下的光功率，横坐标为变化的上波导层In摩尔分数，得到图5(a)。可以看到，光功率随着In摩尔分数的增加先增大后变小，其中In摩尔分数为8%时光功率最高，取该样品为样品B(以下简称为样品B)。此外还分析了这一系列样品在1 A电流注入下，电子溢出至上波导层的电子泄漏率(PELC)，以及电子和空穴基态波函数在空间上的重合率随着In摩尔分数变化的曲线，如图5(b)所示。同样可以看到，泄漏率先快速下降再缓慢回升，在In摩尔分数取8%时泄漏率最低，为18.0%，这意味着在1 A注入电流下注入到量子阱中的电子仅有18%溢出量子阱到达了p型区。电子空穴波函数重合率的变化趋势则与前者相反，先快速上升，在In摩尔分数8%左右最高，这说明此时电子和空穴在空间上的重合度达到极大值，更有利于发生辐射复合，这两者整体与光功率变化的趋势一致。

这一趋势的原因是随着In摩尔分数的增加，电子

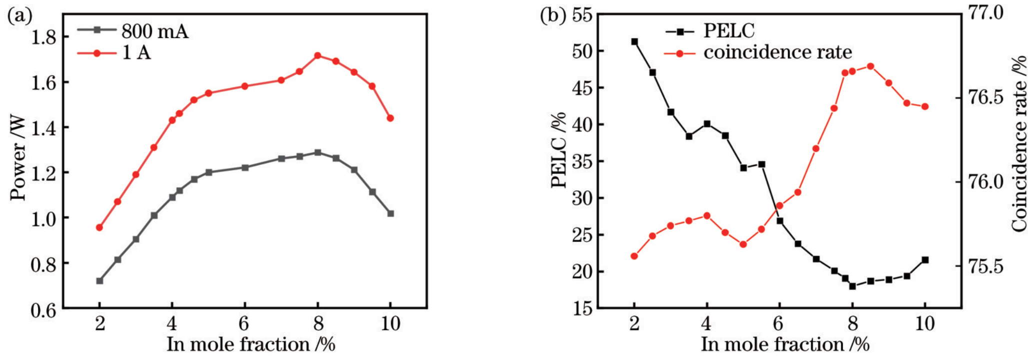

图 5　将标准结构的上波导层 In 摩尔分数改变。(a)不同注入电流下光功率随着 In 摩尔分数变化的曲线;(b)1 A 电流下电子泄漏率和波函数重合率随着 In 摩尔分数变化的曲线

Fig. 5　Standard structure changes with the In mole fraction of UWG layer. (a) Curves of optical power with In mole fraction under different injection currents; (b) curve of electron leakage rate and wave function coincidence rate with In mole fraction at 1 A current

的有效势垒逐渐提升,电子泄漏得到有效改善。但当 In 摩尔分数超过 8% 之后,过高的组分差会导致能带弯曲,界面处积累过多电荷,使电子和空穴发生空间分离,波函数重叠减少。此外,光场也随着 In 摩尔分数增加向 n 区移动,在超过 8% 之后逐渐远离有源区,光场限制因子减小,同样导致出光效率变差。

为了解决组分差过大导致的能带弯曲问题,本文尝试使用渐变组分的上波导结构来缓解这一问题。随后设计了一系列渐变 In 摩尔分数上波导层的蓝光 LD,除波导层 In 摩尔分数以外其他参数与样品 A、样品 B 相同,固定靠近 p 型区一侧的 In 摩尔分数使其与样品 B 相同,改变靠近量子阱一侧的 In 摩尔分数,也就是固定渐变的最终值为 8%,改变渐变的起始值。如图 6 所示,可以看到渐变摩尔分数 5%~8% 的样品光功率更高,之后还进行了多组其他渐变摩尔分数的尝试,最终得到 In 摩尔分数渐变区域由 4% 左右渐变至 9% 左右的几个样品,如 4%~8%、4%~9% 等,光功率相对更高且比较接近,而且均高于样品 B,取其中最好的样品 In$_{0.05\text{-}0.08}$Ga$_{0.95\text{-}0.92}$N 为样品 C(以下简称样品 C)。

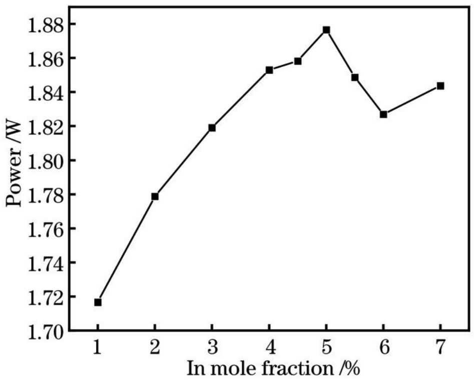

图 6　1 A 电流下光功率随着 In 摩尔分数变化的曲线(改变渐变的起始点)

Fig. 6　Curve of optical power with In mole fraction at 1 A current (change the start point of the gradient)

综合以上三个样品绘制出了 PCE 曲线、光功率曲线如图 7(a)所示,1 A 注入电流下的受激辐射率图如图 7(b)所示,为便于观察,将三个样品的受激辐射合并至一个图中。三条曲线的原始横坐标是重合的。最终分析发现,三者的阈值电流相近,分别为 0.20、0.16、0.19 mA,其中,样品 B 的阈值电流最小,样品 C 由于渐变组分稍有增大,但仍然比样品 A 小。样品 B 的斜率效率达到了 2.09 W/A,相对样品 A 提升了 53.54%,样品 C 的斜率效率为 2.31 W/A,相对样品 A 提升了 69.70%。由于未对样品的电阻造成显著的改动,三者的伏安曲线基本一致,故绘制了 PCE 曲线。其中,样品 A 的最高转化效率为 25.4%,样品 B 则为 43.3%,相对样品 A 提升了 70.47%,样品 C 的最高转化效率达到了 46.1%,相对样品 A 提升了 81.50%。参考受激辐射谱的数值,三个样品的最高峰辐射复合率分别为 7.97×10^{28}、14.85×10^{28}、16.57×10^{28} $\mathrm{cm^{-3}{\cdot}s^{-1}}$,无论是从光电转化效率、斜率效率还是辐射复合率来看,样品 B 和样品 C 都在样品 A 的基础上有相当大的提升,且样品 C 比样品 B 的表现要更好一些。

为了探究新结构性能提升的内在物理机制,分别绘制了三种结构的导带与价带图,图 8(a)为量子阱与上波导层界面处附近的导带图,图 8(b)为此处的价带图。从图 8(a)可以看出,样品 B 和样品 C 都大幅提高了导带电子势垒的高度,相比之前的结构,对电子泄漏有着更明显的抑制作用。由于泄漏的电子在 p 型区会捕获空穴,因而可以减小电子的泄漏率,获得更高的空穴注入量。但在图 8(b)中可以看到,随着上波导层 In 摩尔分数的提高,价带的空穴势垒同样会大幅度提高,这不利于空穴的注入。样品 B 的空穴势垒远高于样品 A 与样品 C,反而降低了空穴注入率。样品 C 则通过 In 摩尔分数的渐变,将电子势垒和空穴势垒的高度都保持在一个合适的状态,因此其最终性能表现也最好。从图 9 的电子电流浓度曲线中也可以得出相同的结论,在图 5(b)中得到样品 A 的电子泄漏率为 51.3%,

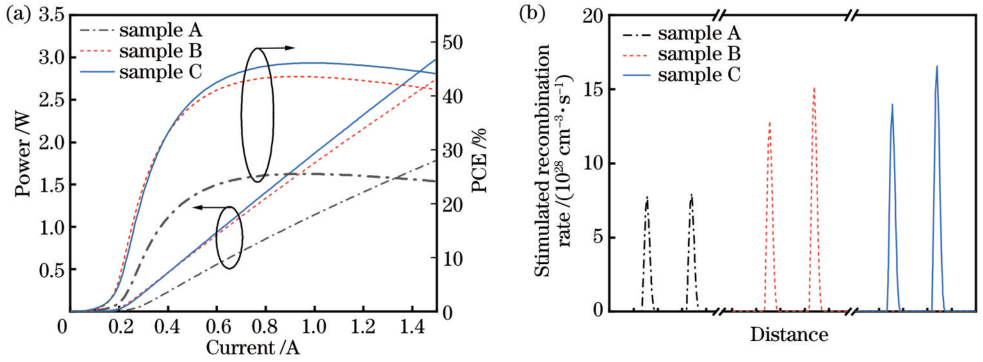

图 7　新结构与标准结构性能。(a)光电转化效率和光功率曲线；(b)受激辐射率对比图

Fig. 7　Performance of the new structure and standard structure. (a) Photoelectric conversion efficiency and optical power curves; (b) comparison of stimulated recombination rate

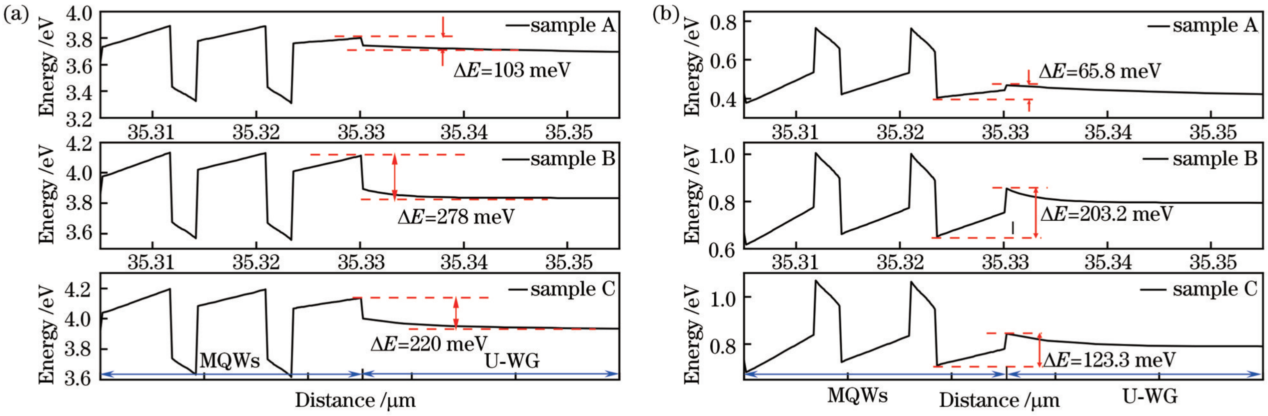

图 8　1 A 电流下三个样品的能带图。(a)导带图；(b)价带图

Fig. 8　Energy band diagrams of three samples at 1 A current. (a) Conduction band; (b) valence band

样品 B 为 18.0%，样品 C 为 13.8%，从结果上证明了渐变的能带优化方案更有利于空穴的注入，抑制电子泄漏。

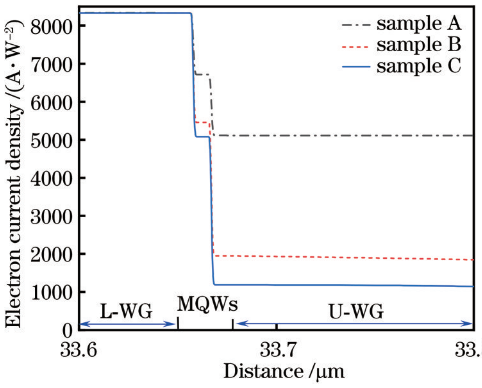

图 9　1 A 电流下三个样品的电子电流密度曲线

Fig. 9　Electron current density curves of three samples at 1 A current

之后在光学层面进行分析，绘制了各自峰值归一化的发光光谱曲线如图 10 所示，三者谱峰位置分别为 445.01、444.97、444.87 nm，相对原始样品最大相对误差也仅有 0.02%，可忽略不计。而三者曲线的半峰全宽（FWHM）如下：样品 A 为 0.28 nm，样品 B 为 0.16 nm，样品 C 为 0.18 nm。两个优化结构都相对样品 A 有更小的半峰全宽，说明光谱的单色性更好，而样品 C 的半峰全宽略大于样品 B，这是因为组分渐变会影响部分禁带宽度，从而影响激光器的单色性。

此外，还绘制了光场分布图，如图 11 所示，可以看到，随着上波导层 In 摩尔分数的增加，上波导层的折

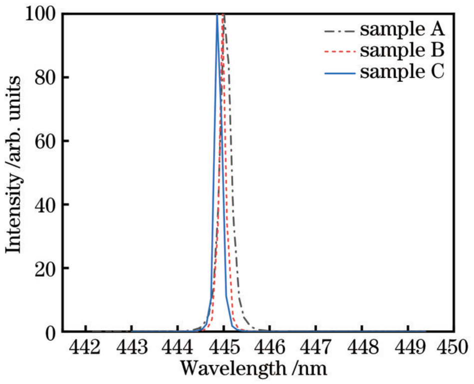

图 10　1 A 电流下三种结构的激射光谱图（各峰值已归一化处理）

Fig. 10　Lasing spectra of three structures at 1 A current (each peak has been normalized)

射率也会增加，导致光场分布向上波导层移动，当In摩尔分数为2%时，光场中心位于下波导层，而在In摩尔分数处于8%的样品B中，光场中心移动到了上波导层，光学限制因子反而下降了。在图5(a)和图5(b)中，当In摩尔分数处于4%左右时，光功率与电子泄漏率都有一个极值，因为此时光场中心恰好位于量子阱，光学限制因子达到最大值，这说明光场位置在影响光功率的若干因素中虽然不是最主要的，但也同样有着重要的作用。而样品C中渐变的上波导层，通过改变材料的组分来改变折射率，光场中心向量子阱移动，有利于将更多的载流子限制在量子阱中受激辐射复合。三者光学限制因子分别为5.89%、5.67%、5.80%，该结果也印证了这一点。

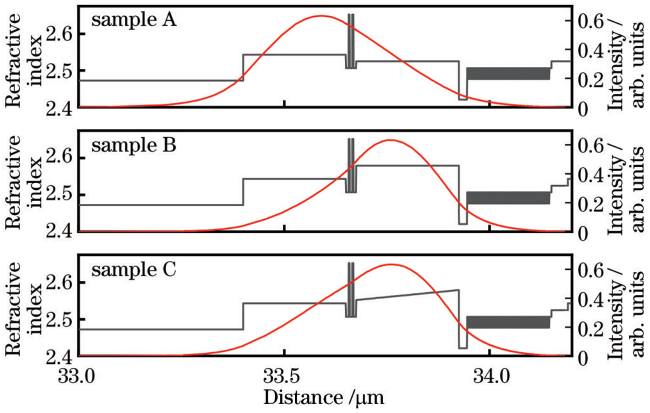

图11　1 A电流下三种结构的光场分布与折射率曲线图

Fig. 11　Optical field distributions and refractive index curves of three structures at 1 A current

4　结　　论

本文基于实验样品结构研究了上波导层不同In摩尔分数对InGaN基蓝光激光器光电效应的影响，并提出了优化器件性能的两种新结构。研究发现，适当提高上波导层的In摩尔分数可以有效减少原结构的载流子泄漏，对输出光功率有显著影响。将原实验结构的上波导层In摩尔分数提升至8%左右，使斜率效率相对原有结构提升了53.54%，在1.5 A的注入电流下达到2.09 W/A。而将上波导层的In摩尔分数改为5%～8%渐变时，可以缓解过高的空穴势垒，进一步促进电子注入，同时光场更加集中，减少了光学损失，使斜率效率相对原有结构提升了69.70%，在1.5 A的注入电流下达到2.31 W/A。

参 考 文 献

[1] 宁永强，陈泳屹，张俊，等．大功率半导体激光器发展及相关技术概述[J]. 光学学报，2021，41(1): 0114001.
Ning Y Q, Chen Y Y, Zhang J, et al. Brief review of development and techniques for high power semiconductor lasers[J]. Acta Optica Sinica, 2021, 41(1): 0114001.

[2] Britten S W, Schmid L, Molitor T, et al. Blue high-power laser sources for processing solutions in e-mobility and beyond[J]. Procedia CIRP, 2020, 94: 592-595.

[3] Qiu P J, Cui G G, Qian Z Y, et al. 4.0 Gbps visible light communication in a foggy environment based on a blue laser diode[J]. Optics Express, 2021, 29(9): 14163-14173.

[4] 孙柳雅，牛明生，陈加雪，等．基于光声光谱技术的NO_2探测[J]. 中国激光，2022，49(23): 2310002.
Sun L Y, Niu M S, Chen J X, et al. Nitrogen dioxide detection based on photoacoustic spectroscopy[J]. Chinese Journal of Lasers, 2022, 49(23): 2310002.

[5] Mehta K, Liu Y S, Wang J L, et al. Theory and design of electron blocking layers for III-N-based laser diodes by numerical simulation[J]. IEEE Journal of Quantum Electronics, 2018, 54(6): 2001310.

[6] 孙天宇，夏明俊，乔雷．半导体激光器失效机理与检测分析研究进展[J]. 激光与光电子学进展，2021，58(19): 1900003.
Sun T Y, Xia M J, Qiao L. Failure mechanism and detection analysis of semiconductor laser[J]. Laser & Optoelectronics Progress, 2021, 58(19): 1900003.

[7] Park S H, Kim H M, Ahn D. Optical gain in GaN quantum well lasers with quaternary AlInGaN barriers[J]. Japanese Journal of Applied Physics, 2005, 44(10R): 7460-7463.

[8] Liu J X, Qie H R, Sun Q A, et al. Enhanced carrier confinement and radiative recombination in GaN-based lasers by tailoring first-barrier doping[J]. Optics Express, 2020, 28(21): 32124-32131.

[9] Liang F, Zhao D G, Liu Z S, et al. Improved performance of GaN-based blue laser diodes using asymmetric multiple quantum wells without the first quantum barrier layer[J]. Optics Express, 2022, 30(6): 9913-9923.

[10] Yang J, Zhao D G, Jiang D S, et al. Enhancing the performance of GaN based LDs by using low in content InGaN instead of GaN as lower waveguide layer[J]. Optics & Laser Technology, 2019, 111: 810-813.

[11] Liang F, Zhao D G, Jiang D S, et al. Improvement of slope efficiency of GaN-Based blue laser diodes by using asymmetric MQW and $In_xGa_{1-x}N$ lower waveguide[J]. Journal of Alloys and Compounds, 2018, 731: 243-247.

[12] Onwukaeme C, Ryu H Y. Investigation of the optimum Mg doping concentration in p-type-doped layers of InGaN blue laser diode structures[J]. Crystals, 2021, 11(11): 1335.

[13] Xing Y, Zhao D G, Jiang D S, et al. Suppression of electron and hole overflow in GaN-based near-ultraviolet laser diodes[J]. Chinese Physics B, 2018, 27(2): 028101.

[14] He L F, Zhang K, Wu H L, et al. Efficient carrier transport for 368 nm ultraviolet LEDs with a p-AlInGaN/AlGaN short-period superlattice electron blocking layer[J]. Journal of Materials Chemistry C, 2021, 9(25):7893-7899.

[15] 杜小娟，刘晶，董海亮，等．电子阻挡层Al组分对GaN基蓝光激光二极管光电性能的影响[J]. 发光学报，2022，43(5): 773-785.
Du X J, Liu J, Dong H L, et al. Effect of Al composition of electron blocking layer on photoelectric performance of GaN-based blue laser diode[J]. Chinese Journal of Luminescence, 2022, 43(5): 773-785.

[16] 胡磊，张立群，刘建平，等．高功率氮化镓基蓝光激光器[J]. 中国激光，2020，47(7): 0701025.
Hu L, Zhang L Q, Liu J P, et al. High power GaN-based blue lasers[J]. Chinese Journal of Lasers, 2020, 47(7): 0701025.

[17] Zhong Z B, Lu S Q, Li J C, et al. Design and fabrication of high power InGaN blue laser diode over 8 W[J]. Optics & Laser Technology, 2021, 139: 106985.

[18] Brendel M, Kruse A, Jönen H, et al. Auger recombination in GaInN/GaN quantum well laser structures[J]. Applied Physics Letters, 2011, 99(3): 031106.

[19] Cai X F, Li S P, Kang J Y. Improved characteristics of ultraviolet AlGaN multiple-quantum-well laser diodes with step-

graded quantum barriers close to waveguide layers[J]. Superlattices and Microstructures, 2016, 97: 1-7.

[20] Sun P, Dang S H, Li T B, et al. Carrier transport improvement in blue InGaN light-emitting diodes via reduced polarization using a band-engineered electron blocking layer[J]. Journal of Display Technology, 2014, 10(12): 1101-1105.

[21] Chen C Y, Hsieh C, Liao C H, et al. Effects of overgrown p-layer on the emission characteristics of the InGaN/GaN quantum wells in a high-indium light-emitting diode[J]. Optics Express, 2012, 20(10): 11321-11335.

[22] Li X, Zhao D G, Jiang D S, et al. The effectiveness of electron blocking layer in InGaN-based laser diodes with different indium content[J]. Physica Status Solidi (a), 2016, 213(8): 2223-2228.

[23] Kuo Y K, Chang J Y, Chen F M, et al. Numerical investigation on the carrier transport characteristics of AlGaN deep-UV light-emitting diodes[J]. IEEE Journal of Quantum Electronics, 2016, 52(4): 3300105.

[24] Kozaki T, Matsumura H, Sugimoto Y, et al. High-power and wide wavelength range GaN-based laser diodes[J]. Proceedings of SPIE, 2006, 6133: 613306.

[25] Morkoç H. Handbook of nitride semiconductors and devices: GaN-based optical and electronic devices[M]. Weinheim: Wiley, 2008.

[26] Vurgaftman I, Meyer J R, Ram-Mohan L R. Band parameters for III-V compound semiconductors and their alloys[J]. Journal of Applied Physics, 2001, 89(11): 5815-5875.

[27] Gaikwad S A, Samuel E P, Patil D S, et al. Theoretical analysis of effect of temperature on threshold parameters and field intensity in GaN material based heterostructure[J]. Bulletin of Materials Science, 2007, 30(3): 255-261.

Effect of In Mole Fraction in Upper Waveguide Layer on Performance of InGaN-Based Blue Lasers

Fu Xingrui, Li Shuping*

College of Physical Science and Technology, Xiamen University, Xiamen 361005, *Fujian, China*

Abstract

Objective To constantly improve performance requirements for InGaN lasers, we investigate the effect of the In mole fractionin the upper waveguide layer on the performance of InGaN-based blue laser diodes. The research results can be employed to improve the performance of InGaN-based blue laser diodes which have many potential applications in areas such as solid-state lighting, laser displays, and optical storage. Our study is motivated by electron leakage limiting the output power of laser diodes. Due to mobility differences, the injection rate of holes will be slower than that of electrons to bring about varying amounts of hole injection in several quantum wells, which makes electrons leak into the waveguide layer and reduces the carrier density in the active layer. Additionally, the polarization effect of InGaN materials will lead to energy band offset and quantum confinement Stark effect. To this end, many optimization ideas have been proposed, but most of them focus on multiple quantum wells and barriers, lower waveguide layers, and electron barrier layers. Our study shows that the upper waveguide layer also plays a crucial role in the performance of InGaN-based blue laser diodes. By adjusting the In mole fraction of the upper waveguide layer, the corresponding band structure can be changed to alleviate the electron current overflowing from the quantum well, thereby improving the radiation recombination rate and optical output.

Methods Based on the experimental sample structure, an InGaN-based blue laser with the same structure is constructed by PICS3D simulation software. Its photoelectric performance, such as the optical power curve, voltammetry curve, and spectral peak curve, achieves strict comparison. The internal parameters are measured in a manner consistent with the experimental sample. In the reference, the reflectivity of the front cavity surface is modified to 10%, 45%, and 82% in turn, and different slope efficiencies are obtained. The internal loss and carrier injection rate of the laser are indirectly measured by linear fitting. We also adopt the same setting parameters, measure internal parameters in the same way, and compare them with references. It is found that the relative errors of internal loss and carrier injection efficiency are 3.5% and 5.3%, which proves the reliability of subsequent data in our paper. Subsequently, a series of InGaN-based blue lasers are constructed, and the In mole fraction in the upper waveguide layer is optimized by comparing the optical output power, carrier distribution, optical field distribution, radiation recombination coefficient, and energy band curve parameters under different In contents. During employing a constant In component, we find that as the In mole fraction increases, the effective potential barrier to electrons gradually rises, with improved electron leakage. However, when the In mole fraction exceeds 8%, the high component difference will lead to bending energy bands and accumulated excessive charges at the interface, which will cause space separation of electrons and holes, and the wave function overlap will be reduced. In addition, with the rising In mole fraction, the light field also moves away from the active region, thereby resulting in a decrease in the light field limiting factor and a decrease in light output efficiency. Therefore, a series of InGaN-based blue light lasers with gradient components are constructed, and the optimal gradient component is obtained through comprehensive comparison.

Results and Discussions Firstly, the original sample with strictly consistent parameters and structure is set according to the references, and its optical power curve and wavelength are also consistent with the experimental sample (Fig. 2). The internal loss is measured by adopting the same variable cavity surface method as the experimental process (Fig. 3), which is compared with the references and shows credibility. Secondly, the optical power, electron leakage rate, and wave function coincidence rate of the upper waveguide layer with different constant In contents are compared (Fig. 5). Subsequently, a series of gradient component upper waveguide structures are constructed with fixed final values of the gradient, the initial value of the gradient is changed, and their optical power is compared (Fig. 6). Finally, two different optimized structures with better optical power have been proposed, and both of them reduce electronic leakage and improve slope efficiency, thereby enhancing photoelectric conversion efficiency (Fig. 7). The sample with gradient components has the most suitable height of electron and hole barriers, thus leading to a higher hole injection amount. In terms of optics, our proposed sample changes the refractive index of the material through a gradient upper waveguide layer, which makes the center of the light field move towards the active region (Fig. 11) and is conducive to limiting more carriers to the stimulated radiation recombination in the quantum well.

Conclusions We investigate the effect of the In mole fraction in the upper waveguide layer on the performance of InGaN-based blue laser diodes. The results show that appropriately increasing the In mole fraction of the upper waveguide layer can reduce the carrier leakage of the original structure, which exerts a significant influence on the output optical power. The In mole fraction in the upper waveguide layer of the original experimental structure is increased to about 8%, and then the slope efficiency rises by 53.54% of the original value and reaches 2.09 W/A at 1.5 A injection current. When the In mole fraction of the upper waveguide layer is changed to 5%-8%, the high hole barrier can be alleviated, with improved electron injection. Meanwhile, the optical field is more concentrated and the optical loss is reduced. The slope efficiency is increased by 69.70% compared with the original structure and reaches 2.31 W/A at 1.5 A injection current. The research results provide valuable references for the design and fabrication of high-performance InGaN-based blue laser diodes.

Key words diode lasers; upper waveguide layer; gradient layer; electronic leakage